Struct Multidisc Optim (2006) 32: 229–240
DOI 10.1007/s00158-006-0019-9

RESEARCH PAPER

E. A. Fancello

Topology optimization for minimum mass design considering local failure constraints and contact boundary conditions

Received: 2 August 2005 / Revised manuscript received: 3 January 2006 / Published online: 8 July 2006
© Springer-Verlag 2006

Abstract The purpose of this work is to present a possible approach to the topology mass minimization of a body submitted to local material failure constraints, contact boundary conditions, and multiple load cases. The formulation combines the well-known SIMP approach (Solid Isotropic Microstructure with intermediate mass Penalization) and the Augmented Lagrangian technique to deal with stress-based constraints. At every design step and load case, a contact solver is called to obtain the equilibrium deformed configuration. Assuming differentiability, the sensitivity analysis is performed analytically at the cost of a Newton iteration. Finally, some numerical examples are presented to explore the differences and similarities found in the final designs for this case and for the case of minimization of internal energy, also with contact boundary conditions.

1 Introduction

A brief search in the literature will show that the problem of structural topology optimization considering local failure constraints has received much less attention than the classic compliance problem. One of the most important reasons for this is the difficulty introduced by the local constraints. First, a great number of constraints are usually needed due to their local nature. Second, when approaches like SIMP or homogenization are used, the continuous design variable (for example, density) may go to zero and enforce the failure function to reach unreasonable values. This characterizes the phenomenon called *Singularity Stress*. Pioneer works dealing with this phenomenon were developed by Sved and Ginos (1968), Kirsch (1990), and Cheng and Guo (1997). The main contribution of the latter work is the incorporation of a regularization factor that modifies the design and makes it regular, allowing the use of ordinary mathematical programming algorithms. The extension of these ideas to the case of continuum structures is seen in Duysinx and Bendsøe (1998) and Duysinx and Sigmund (1998).

In Pereira et al. (2004), a similar theoretical background to that of Duysinx and Bendsøe (1998) is used in combination with a penalization-type (Augmented Lagrangian) approach to deal with stress constraints, obtaining quite satisfactory numerical results. Also, in Fancello and Pereira (2003), this approach is extended to handle multiple-load conditions. The problems arising from this latter study motivated the present one. In mechanical devices, the existence of contact conditions is common. In this case, different loads usually activate different regions of the contact boundary to satisfy equilibrium.

Optimization of structures submitted to contact boundary conditions has been the subject of intensive investigation [see, among many other references, the book by Haslinger and Neittaanmäki (1996), the paper by Sokolowski and Zolesio (1987), the review by Hilding et al. (1999) and references therein]. Contributions by the current author to the field can be found in Fancello and Feijóo (1994) and Fancello et al. (1995). Theoretical and numerical studies on topology optimization of sheets with unilateral contact conditions are reported in Petersson (1996), Petersson and Patriksson (1997), and Petersson and Haslinger (1998) where the focused problem is the maximization of stiffness.

This paper addresses the problem of topology optimization of continuum bodies with contact boundary conditions searching for minimum mass design with local failure (stress) constraints.

An outline of the formulation and its numerical approach is presented in the Sections 2 to 6. In Section 7, some examples are shown comparing the solutions of the proposed problem with those obtained by the minimization of strain energy subject to volume constraints and contact boundary conditions.

Finally, Section 8 contributes to the discussion about the benefits and drawbacks of the present formulation. Some particular remarks were left to this last section with the purpose of emphasizing their relationship with the information provided by the numerical examples.

E. A. Fancello (✉)
Departamento de Engenharia Mecânica,
Universidade Federal de Santa Catarina, Santa Catarina, Brazil
e-mail: fancello@grante.ufsc.br

2 Contact problem

Consider the contact problem with Coulomb friction. Consider also a penalization approach to the unilateral condition and the inclusion of an elastic reversible term for the tangential displacements (or velocities). The variational problem may be set as searching for the displacement field $\mathbf{u} \in \mathcal{K}$ such that

$$B(\mathbf{u}, \mathbf{v}) - l(\mathbf{v}) - l_c(\mathbf{u}, \mathbf{v}) = 0 \quad \forall \mathbf{v} \in \mathcal{V}, \tag{1}$$

$$B(\mathbf{u}, \mathbf{v}) = \int_\Omega \mathbf{D} \nabla \mathbf{u}^s \cdot \nabla \mathbf{v}^s \, d\Omega, \tag{2}$$

$$l(\mathbf{v}) = \int_\Omega \mathbf{b} \cdot \mathbf{v} \, d\Omega + \int_{\Gamma_f} \mathbf{f} \cdot \mathbf{v} \, d\Gamma, \tag{3}$$

$$l_c(\mathbf{u}, \mathbf{v}) = \int_{\Gamma_c} (t_N(\mathbf{u}) v_N + \mathbf{t}_T(\mathbf{u}) \cdot \mathbf{v}_T) \, d\Gamma. \tag{4}$$

The sets $\mathcal{K}$ and $\mathcal{V}$ define the kinematically admissible set of displacements and variations, respectively. The first two terms of (1) are the bilinear form B and linear form l representing the virtual work of internal and external forces, $\mathbf{D}$ is the elasticity tensor and $\nabla \mathbf{u}^s$ is the symmetric gradient of real displacements.

Body forces $\mathbf{b}$ are applied over Ω, while known traction forces $\mathbf{f}$ are set on the portion of the boundary called Γ_f. The last term of (1) computes the virtual work of normal and tangential contact forces $(t_N, \mathbf{t}_T)$ applied on the portion Γ_c of the boundary, also called contact boundary (see Fig. 1a). The value of the contact forces depends on the displacements and velocities of points of Γ_c through of tribological laws. Among other possible formulations, the following classical set of equations defines a unilateral contact interface condition with Coulomb friction:

$$u_n = \mathbf{u} \cdot \mathbf{n}, \quad \mathbf{u}_T = \mathbf{u} - u_n \mathbf{n}, \quad g = u_n - s, \tag{5}$$

$$t_N(\mathbf{u}) = k_N \, \langle g(\mathbf{u}) \rangle = k_N \, \langle u_n - s \rangle \,, \tag{6}$$

$$\dot{\mathbf{u}}_T = \dot{\mathbf{u}}_T^e + \dot{\mathbf{u}}_T^s, \quad \dot{\mathbf{u}}_T^s = -\dot{\xi} \, \frac{\partial \phi}{\partial \mathbf{t}_T}, \tag{7}$$

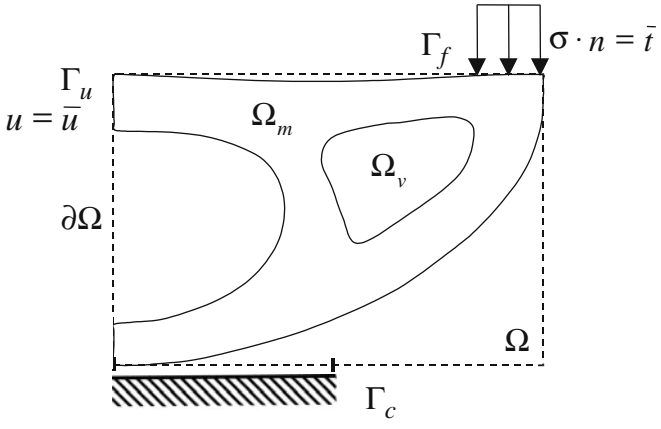

Fig. 1 Domain composed of solid, voids, and contact boundary

$$\dot{\mathbf{t}}_T = -k_T \dot{\mathbf{u}}_T^e = -k_T (\dot{\mathbf{u}}_T - \dot{\mathbf{u}}_T^s), \tag{8}$$

$$\phi = \|\mathbf{t}_T\| + \mu t_N \leq 0, \quad \dot{\xi} \geq 0, \quad \dot{\xi} \, \phi = 0. \tag{9}$$

Equation (5) defines normal and tangential displacements of the contact boundary through projections of the displacement $\mathbf{u}$ on the boundary normal $\mathbf{n}$. The function g is the actual gap between two bodies in contact while s is the initial gap. A penalization-type constitutive equation for normal traction is given by (6), where the Heaviside operator $\langle \cdot \rangle$ takes the positive value of the argument. Tangential velocities are split into elastic and sliding components (7). Moreover, the relationship between tangential displacements and tractions follows expressions analogous to those of perfect elastoplasticity. Tangential traction rates depend on the elastic part of the tangential velocities. The sliding velocity is given by (7), i.e., it is proportional to the derivative of a sliding potential ϕ defined by (9) (Coulomb model). Considering the solution for time step j to be completely known, the weak equilibrium expression at time $j+1$ is given by Simo and Laursen (1992):

$$B(\mathbf{u}^{j+1}, \mathbf{v}) - l^{j+1}(\mathbf{v}) - l_c(\mathbf{u}^{j+1}, \mathbf{v}) d\Gamma = 0 \quad \forall \mathbf{v} \in \mathcal{V}. \tag{10}$$

A discrete version of (10) can be obtained by using conventional finite elements. Moreover, different approaches may be used to discretize the integral equations along the contact boundary (e.g., Wriggers et al. 1990). The most straightforward form of solving (10) is using the Newton method with a tangent matrix computed by the derivative of the residual with respect to displacements. Considering that external forces are independent of displacements, the equilibrium of the structure can be posed by the classical expression

$$\mathbf{R}^k = \mathbf{R}(\mathbf{U}^k) = \mathbf{F}_{int} - \mathbf{F}_{ext} - \mathbf{F}_{cN} - \mathbf{F}_{cT}, \tag{11}$$

$$\mathbf{K}^k = \frac{\partial \mathbf{R}^k}{\partial \mathbf{U}} = \mathbf{K}_{int} - \mathbf{K}_N - \mathbf{K}_T. \tag{12}$$

The residual $\mathbf{R}^k$ in (11) is composed of internal forces, external forces (produced by $\mathbf{b}$ and $\mathbf{f}$) and contact forces, split into normal and tangential parts. The consistent matrices $\mathbf{K}_N$ and $\mathbf{K}_T$ in (12) are obtained by deriving the contact forces in (11) with respect to displacement parameters $\mathbf{U}$. It is worth mentioning that, due to the coupling between normal and tangential tractions in the friction behavior, the consistent matrix $\mathbf{K}_T$ is (in the present approach) not symmetric.

It is well-known that pure penalization treatment for contact condition leads to numerical ill-conditioning. To overcome this inconvenience, Augmented Lagrangian formulation is usually included for both normal and tangential contact behavior. This inclusion, however, does not modify the regularization approach concept of (5–9) and we will remain with these expressions for clarity reasons.

To end this section, we highlight that the converged tangential consistent matrix $\mathbf{K}^k$ (i.e., the one obtained at the solution of the nonlinear problem) plays an important role in the computation of the sensitivity equations for the optimization problem.

3 Optimization problem

Consider the body defined in the previous section where the material part Ω_m and the void region Ω_v of Ω (see Fig. 1b) can be distinguished. The problem focused in this paper is the minimization of the body mass subject to local failure constraints and, for the purpose of clarity, it will be referenced along this paper as the *minimum mass problem*. Then, for a given domain Ω, the optimization problem to be solved is

Minimize Mass

$$\text{Subject to : } \mathrm{F_i}\left(\sigma_{\mathrm{i}}\left(\mathbf{x}\right)\right) \leq 0, \quad \forall\ \mathbf{x} \in \Omega, \quad \mathrm{i} = 1...\mathrm{N}, \tag{13}$$

where F_i is a material failure function related to the stress field $\sigma_i\left(\mathbf{x}\right)$ in equilibrium with the corresponding i-th load case. N is the number of load cases. It is well-known that (13) is ill-posed and its direct treatment is, therefore, not appropriate. Among several techniques used to circumvent this problem, the SIMP artificial microstructure defines a relative density ρ that controls the elastic constitutive equation through the following expression:

$$\mathbf{D}_\rho = f_D\left(\rho\right)\mathbf{D} = \rho^p\mathbf{D}, \tag{14}$$

$$\sigma \ \ = \mathbf{D}_\rho\varepsilon, \quad \bar{\sigma} = \mathbf{D}\,\varepsilon. \tag{15}$$

The effective stress tensor $\bar{\sigma}$ for an arbitrary intermediate material depends on the original (solid material) elasticity tensor and the apparent (homogenized) value of deformation (Duysinx and Bendsøe 1998). An appropriate definition of the effective stress $\bar{\sigma}$ is a key aspect in the present problem due to its relation with the failure function. A different approach to defining this effective stress is given in Allaire et al. (2004) in the context of homogenized microstructures. For a given effective stress tensor $\bar{\sigma}$, an equivalent (von Mises) scalar stress σ_e is computed and a failure function is defined:

$$F\left(\bar{\sigma}\right) = \frac{\sigma_e}{\sigma_{adm}} - 1 \leq 0, \tag{16}$$

where σ_{adm} is the material yielding stress or maximum admissible value. To overcome the *Stress Singularity* phenomenon, the ϵ-regularization technique (Cheng and Guo 1997) is used and the failure function is re-defined:

$$\begin{cases} g\left(\mathbf{x}\right) \equiv \rho\left(\mathbf{x}\right) F\left(\bar{\sigma}\left(\mathbf{x}\right)\right) \\ \qquad -\epsilon\left(1-\rho\left(\mathbf{x}\right)\right) \leq 0, \qquad a.e.\ in\ \Omega, \\ 0 < \epsilon^2 = \rho_{\min} \leq \rho\left(\mathbf{x}\right) \leq 1, \qquad \forall\ \mathbf{x} \in \Omega. \end{cases} \tag{17}$$

The optimization problem is then posed as the minimization of the functional $m\left(\rho\right)$ subject to a set of local failure constraints:

$$\underset{\rho \in W_\rho^{1,2}(\Omega)}{\mathrm{Min}}\ m\left(\rho\right) = \int_\Omega \rho\, d\Omega + \frac{1}{2} r_\rho \int_\Omega f_\rho\left(\rho\right)\, d\Omega + r_m \int_\Omega f_m\left(\rho\right)\, d\Omega \tag{18}$$

$$\text{s.t.} \quad g_i\left(\mathbf{x}\right) = g\left(\rho\left(\mathbf{x}\right), \bar{\sigma}_i\left(\mathbf{x}\right)\right) \leq 0, \quad i = 1...N, \tag{19}$$

where

$$f_\rho\left(\rho\right) = \left(\nabla\rho\right)^T\left(\nabla\rho\right), \tag{20}$$

$$f_m\left(\rho\right) = \rho(1-\rho), \tag{21}$$

$$W_\rho^{1,2}\left(\Omega\right) = \left\{ \begin{array}{c} \rho \mid \rho \in W^{1,2}\left(\Omega\right); \\ 0 < \rho_{\min} \leq \rho(\mathbf{x}) \leq 1\ \ \forall\ \mathbf{x} \in \Omega \end{array} \right\}. \tag{22}$$

The checkerboard phenomenon is controlled by the second term of $m\left(\rho\right)$, which is a penalization of the density gradients. The third term introduces an explicit penalization of the intermediate densities. Constants r_m and r_ρ are the corresponding penalization factors.

Aiming to obtain numerical solutions, a classic Augmented Lagrangian functional is defined by introducing the stress constraints as penalization terms into the cost function. Defining $g_i\left(\rho, \bar{\sigma}\right)$, we can write the Augmented Lagrangian function as

$$\pounds\left(\rho; \lambda, \mathbf{r}\right) = m\left(\rho\right) + \sum_{i=1}^{N} m_i\left(\rho; \lambda_i, r_i\right) \tag{23}$$

$$= m\left(\rho\right) + \sum_{i=1}^{N} \int_\Omega M\left(\rho; \lambda_i, r_i\right) d\Omega, \tag{24}$$

$$M\left(\rho; \lambda_i, r_i\right) d\Omega = \frac{1}{r_i} \max\left\{ g_i\left[\lambda_i r_i + \frac{1}{2} g_i\right]; -\frac{\left(r_i\lambda_i\right)^2}{2} \right\}. \tag{25}$$

The penalization functional $m_i\left(\rho; \lambda_i, r_i\right)$ for the i-th load case consists of linear and quadratic terms of the failure function g_i that are multiplied by a penalization parameter $r_i > 0$ and by a Lagrangian function $\lambda_i \in L^2\left(\Omega\right)$. Thus, for a given set $\mathbf{r}^k = \{r_1^k, r_2^k, ..., r_N^k\} > 0$ and $\lambda^k = \{\lambda_1^k, \lambda_2^k, ..., \lambda_N^k\}$, $\lambda_i^k, \in L^2\left(\Omega\right)$, the following box-constrained problem can be solved for each k-th iteration:

$$\underset{\rho \in W_\rho^{1,2}(\Omega)}{\mathrm{Min}}\ \pounds\left(\rho; \lambda^k, \mathbf{r}^k\right). \tag{26}$$

The solution of the whole optimization problem is obtained by solving a sequence of subproblems (26) with an appropriate updating of parameters λ^k, $\mathbf{r}^k$. In this approach, the standard Augmented Lagrangian updating rule has been chosen (for a review, see Bertsekas 1996):

$$\lambda_i^{k+1} = \max\left\{ \lambda_{\mathrm{i}}^{\mathrm{k}} + \frac{1}{2}\mathrm{g_i}\,;\, 0 \right\}, \quad \mathrm{r_i^{k+1}} = \frac{\mathrm{r_i^{k+1}}}{\mathrm{t}}, \quad \mathrm{t} > 1. \tag{27}$$

4 Sensitivity analysis

The algorithm chosen to solve problem (26) needs information of first-order derivatives of the Lagrangian functional. It is well-known that the solution $\mathbf{u}$ to the equilibrium problem is, in general, not differentiable with respect to design variables (e.g., size, shape). The non-differentiable

designs are those in which, at the equilibrium configuration, the set of points not satisfying strict complementarity $\{x \in \Gamma_c : g(x) = 0, \quad t_N(x) = 0\}$ contains an open non-empty subset (Sokolowski and Zolesio 1987). Even so, we assume that this condition is not frequent in practical finite computations, which allow us to use the classical analytical formalism to compute the derivatives. On the other hand, the lack of differentiability of the solution $\mathbf{u}$ is related to the fact that, numerically, the introduction of a new node in effective contact changes the sensitivity values of the problem, driving it to a local solution associated with that contact distribution. Hilding (2000) presents simple examples to illustrate this subject and proposes a heuristic approach to reduce the chances of achieving undesirable local solutions.

Detailed operations to obtain analytical expressions of the gradients are found in Pereira et al. (2004). The directional (Gateaux) derivative of the objective functional $\pounds\left(\rho; \lambda^k, \mathbf{r}^k\right)$ for fixed and known values of λ^k and $\mathbf{r}^k$ is given by:

$$\dot{\pounds}\left(\rho; \lambda^k, \mathbf{r}^k\right)[y] = \dot{m}(\rho)[y] + \sum_{i=1}^{N} \dot{m}_i\left(\rho; \lambda_i^k, r_i^k\right)[y], \quad (28)$$

where

$$\dot{m}(\rho)[y] = \int_\Omega \left[1 + r_m \frac{df_m(\rho)}{d\rho} + \frac{1}{2} r_\rho \frac{df_\rho(\rho)}{d\rho}\right] y \, d\Omega, \quad (29)$$

$$\dot{m}_i\left(\rho; \lambda_i^k, r_i^k\right)[y] = m_i'\left(\rho; \lambda_i^k, r_i^k\right)[y] - B'(\mathbf{u}_i, \mathbf{u}_i^a)[y] + l'(\mathbf{u}_i^a)[y], \quad (30)$$

$$m_i'\left(\rho; \lambda_i^k, r_i^k\right)[y] = \int_\Omega \frac{\partial M_\sigma\left(\rho; \lambda_i^k, r_i^k\right)}{\partial \rho} \, y \, d\Omega, \quad (31)$$

$$\frac{\partial M_\sigma\left(\rho; \lambda_i^k, r_i^k\right)}{\partial \rho} = \frac{1}{r_i^k}\left[F(\sigma_i) + \epsilon\right]\left\langle g_i + r_i^k \lambda_i^k \right\rangle^+. \quad (32)$$

In these expressions, y is a variation of ρ, $\mathbf{u}_i$ is the displacement field for the i-th load case, and $\mathbf{u}_i^a$ is the adjoint solution for the i-th adjoint problem associated with the corresponding load case. The operator $\langle\cdot\rangle^+$ returns the positive value of the argument. The first term, $m(\rho)$, depends explicitly on density ρ, and obtaining its derivative is straightforward. The penalization terms $m_i\left(\rho; \lambda_i^k, r_i^k\right)$ are implicitly dependent on ρ through the mechanical solutions $\mathbf{u}_i(\rho)$ for each load case. Their derivatives are obtained by the adjoint method. The partial (Gateaux) derivative of a for fixed real displacements $\mathbf{u}_i$ and the adjoint solution $\mathbf{u}_i^a$ is given by

$$B'\left(\mathbf{u}_i, \mathbf{u}_i^a\right)[y] = \lim_{t \to 0}\left[\frac{B_{\rho+ty}\left(\mathbf{u}_i, \mathbf{u}_i^a\right) - B_\rho\left(\mathbf{u}_i, \mathbf{u}_i^a\right)}{t}\right] = \int_\Omega q\rho^{(q-1)}\left[\mathbf{D}\nabla^S \mathbf{u}_i \cdot \nabla^S \mathbf{u}_i^a\right] \, y \, d\Omega. \quad (33)$$

Furthermore, it is assumed that external loads do not depend on ρ and, thus, $l_i'\left(\mathbf{u}_i^a\right)[y] = 0$. The solution $\mathbf{u}_i^a$ is computed from the expression of the adjoint problem considering contact conditions:

$$B\left(\mathbf{u}_i^a, \mathbf{v}\right) - \int_{\Gamma_c}\left(\frac{\partial t_N}{\partial \mathbf{u}}^T \mathbf{u}_{i\,\mathrm{N}}^a + \frac{\partial \mathbf{t}_T}{\partial \mathbf{u}}^T \mathbf{u}_{i\,\mathrm{T}}^a\right) \cdot \mathbf{v} \, d\Gamma = \int_\Omega \left(\frac{\partial M_i}{\partial \nabla^S \mathbf{u}} \cdot \nabla^S \mathbf{v}\right) d\Omega, \quad \forall \mathbf{v} \in V, \quad (34)$$

$$= \int_\Omega \left(\frac{\rho}{r_i^k}\left\langle g_i(\mathbf{x}) + r_i^k \lambda_i^k \right\rangle^+ H^{\sigma i} \cdot \nabla^S \mathbf{v}\right) d\Omega, \quad \forall \mathbf{v} \in V, \quad (35)$$

where $H^{\sigma i}$ is a second-order tensor obtained explicitly from the material failure criterion evaluated for the current stress state $\sigma_i = \sigma(\mathbf{u}_i)$. It is worth mentioning that (35) is linear, once the solution of the contact problem $\mathbf{u}_i^a$ is given. The discrete version of the right-hand-side of this last equation gives the tangent matrix $\mathbf{K}$ of (12). Thus, the computation of the derivatives is equivalent to a Newton iteration of the non-linear problem.

5 Minimization of strain energy

It is interesting to compare final designs obtained from the present approach with those obtained from a more classical one like, for example, strain energy minimization with volume constraint. To avoid misinterpretations, this last problem will be referenced in the context of this paper as the *minimum strain energy problem*, which may be stated as

$$\min_{\rho \in W_\rho^{1,2}(\Omega)} \psi(\rho) = \frac{1}{2}\sum_{i=1}^{N} w_i \int_\Omega \mathbf{C}_\rho \nabla \mathbf{u}_i^s \cdot \nabla \mathbf{u}_i^s \, d\Omega,$$

$$\text{subject to :} \quad \underline{V} \le \int_\Omega \rho \, \mathrm{d}\Omega,$$

where $\mathbf{u}_i(\rho)$ is the solution of the equilibrium problem for the i-th load case. It is worth noting that, in this usual formu-

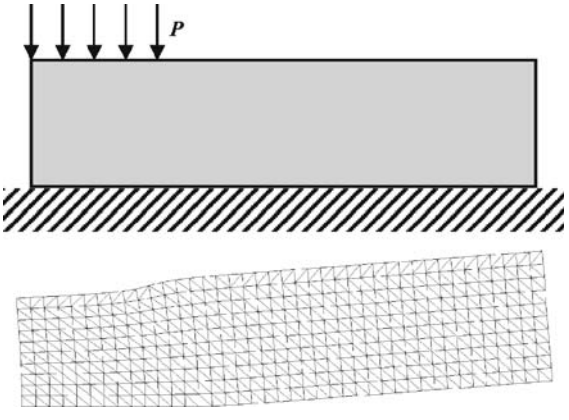

Fig. 2 Block model and deformed mesh for original configuration

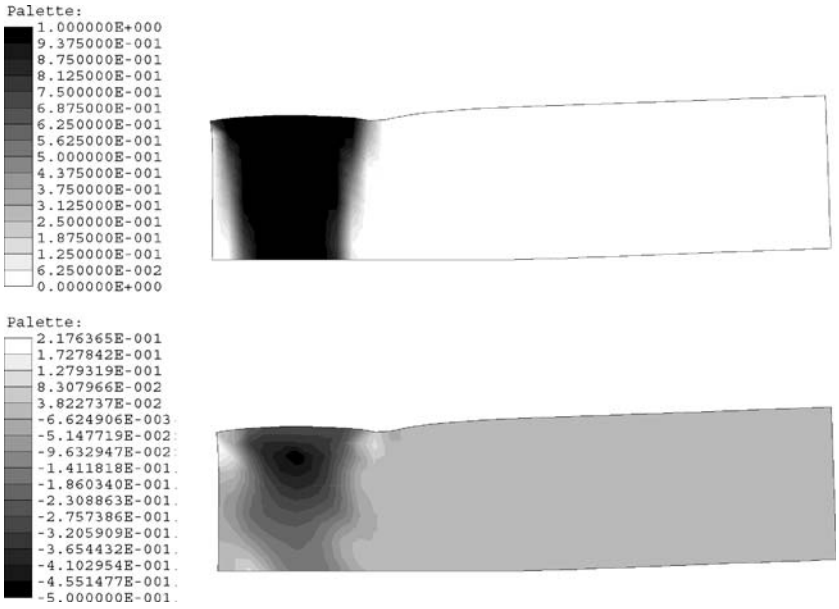

Fig. 3 Strain energy approach. Final design and ε-failure-function distribution

lation, multiple-load cases modify the cost function through the user dependent weighting factors w_i. In contrast to this, the mass minimization problem allows multiple-load cases just by increasing the number of failure constraints.

The solution to this problem may be obtained by following the same basic procedures already shown for the previous case. Sensitivity analysis, if differentiability is assumed, is calculated analytically based on adjoint expressions. Moreover, the simplicity of the single-volume constraint (in contrast with the stress constraints) can be treated either by the already used Augmented Lagrangian technique or by other direct procedures for constraint minimization.

6 Discretization and numerical procedure

The present implementation is limited to 2D problems although the formulation holds for 3D problems. Three-node Lagrangian elements have been used to solve the contact problem and the failure function is evaluated at each element centroid. The same linear-shape functions are used to define a continuous density field ρ, which allow immediate computation of the density gradient penalization term for checkerboard stabilization. Due to these choices, the number of design variables is equal to the number of nodes, while

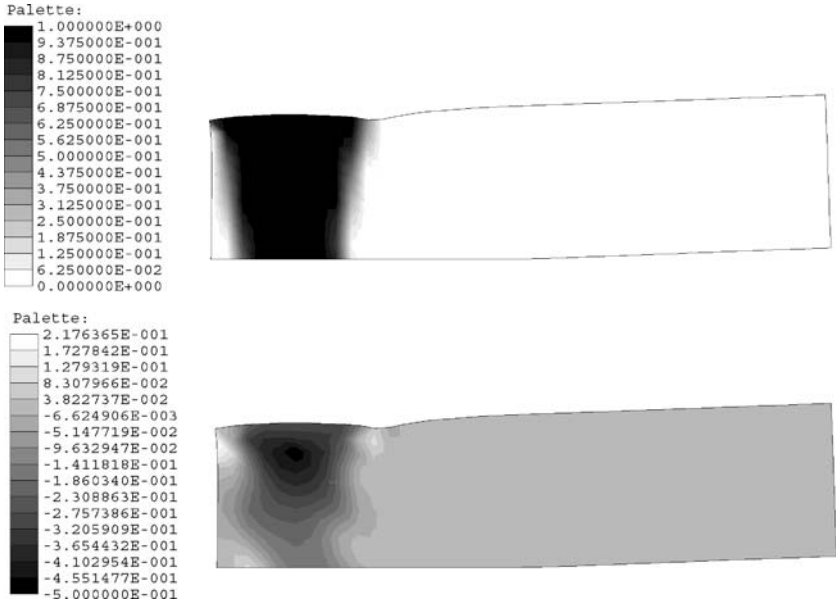

Fig. 4 Minimum mass approach. Final design and ε-failure-function distribution

the number of failure constraints is equal to the number of elements times the number of load cases considered.

The Augmented Lagrangian procedure is used for both the contact problem and the design optimization problem, although we must note that these two stages are completely separate.

In the nonlinear contact problem, an initial set of Lagrangian multipliers representing the contact reactions is defined (usually equal to zero) and a penalization problem is solved. Next, the Lagrangian multipliers are updated by using a conventional rule (Bertsekas 1996), and the sequence is repeated until the complementarity contact conditions are satisfied. It is worth noting that conventional penalization or other techniques for the contact problem may be used without changing the general idea of the present approach.

In the design optimization problem, a set of Lagrangian multipliers and penalization factors $(\lambda^k, \mathbf{r}^k)$ is defined at the k-th subproblem and the minimization of the objective functional $\pounds(\rho; \lambda^k, \mathbf{r}^k)$ subject to side constraints is performed. The sequence of operations is enumerated below:

1. Define $k = 0$, r_m, r_ρ, λ^k and $\mathbf{r}^k$;
2. Minimize the functional $\pounds\left(\rho; \lambda^k, \mathbf{r}^k\right)$, $0 < \rho_{\min} \leq \rho\,(\mathbf{x}) \leq 1$;
3. Verify convergence within a tolerance. If satisfied, stop the process;

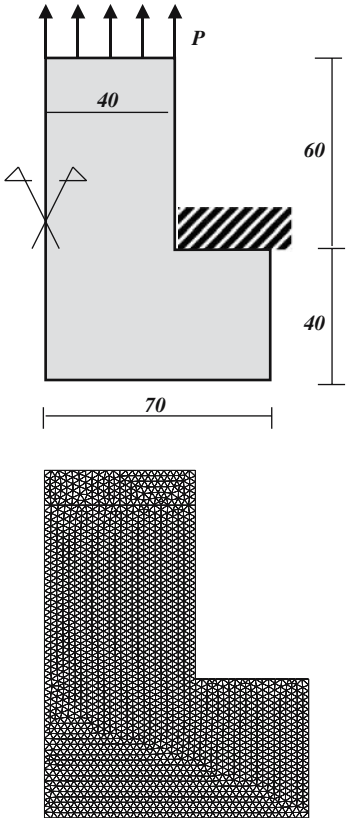

Fig. 5 L-shaped test

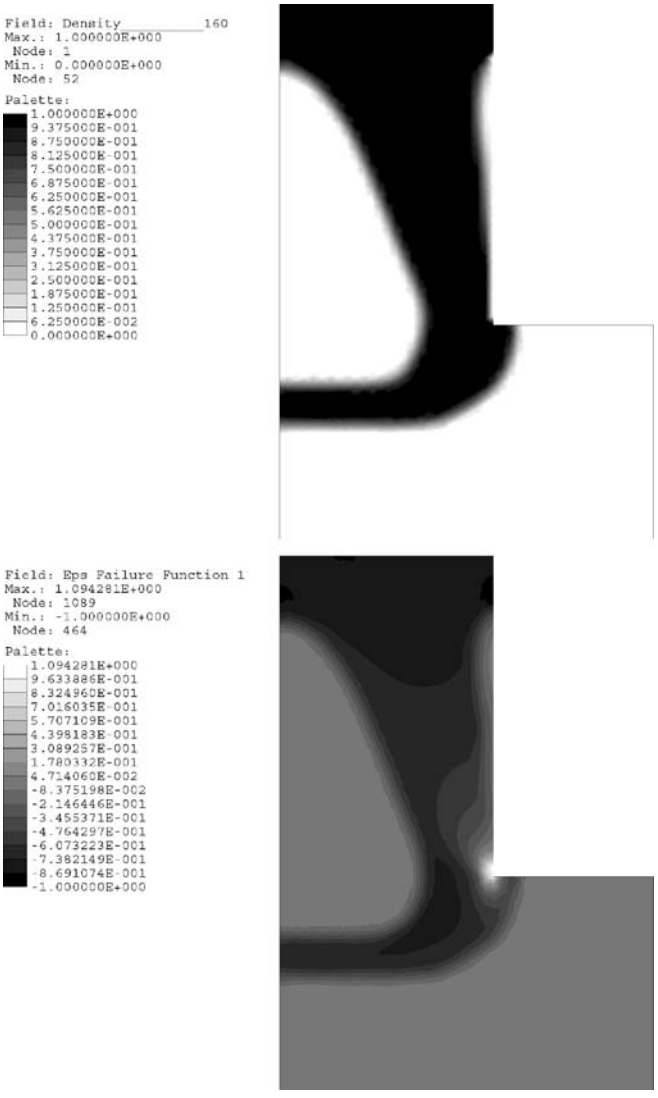

Fig. 6 Strain energy approach. Final design and ε-failure-function distribution

4. Update η^k, λ^k, $\mathbf{r}^k$;
5. $k = k + 1$, return to Step 2.

The optimization algorithm used in Step 2 is a nonlinear trust-region algorithm proposed by Friedlander et al. (1994). This algorithm is based on the construction of a quadratic subproblem defined in a trust region. The results of the present study are obtained with an implementation of this algorithm, called BOX-QUACAN, provided by its authors and parametrically adapted to the present case.

7 Numerical results

Some examples are shown in this paper, aiming to show the behavior of the focused problem, *mass minimization with local failure constraints*, and to compare it with a more com-

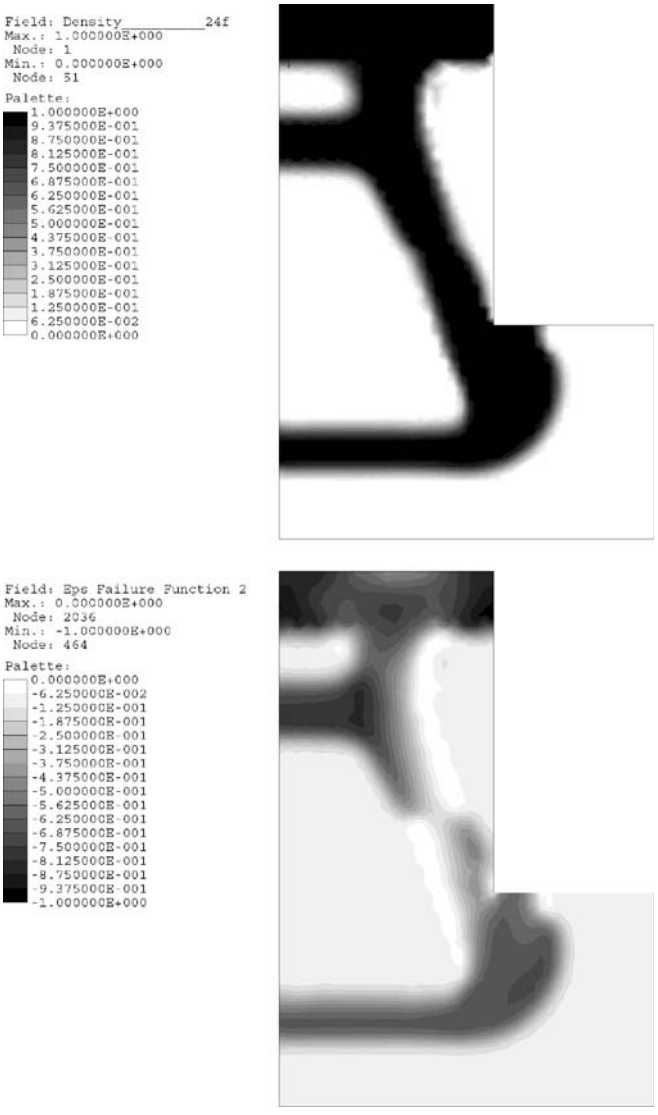

Fig. 7 Minimum mass approach. Final design and ε-failure-function distribution

mon approach, *strain energy minimization with mass constraint*, both of them including contact frictionless boundary conditions. All examples include representations of the final density field with a gray scale varying from 0 (white) to 1 (black) and representations of the failure function given by expression (16) with a gray scale varying from 0 (black) to a positive number (white). It is important to note that the failure constraint is not satisfied in regions having a function value greater than one.

7.1 Block under compression

This simple example shows a case of an elastic block submitted to a pressure on one side of its upper boundary (see Fig. 2). It is possible to see in Figs. 3 and 4 that both approaches provide quite similar shapes. In fact, this example is analogous to that of a tractioned bar in linear elasticity; the tendency for both approaches in this example is to reach a fully stressed design condition in the region far enough from the load application. However, close to the boundary where loads are applied, the shape is slightly different, which makes the strain energy design to have some small failure regions. Dimensions of the block: $40 \times 10 \times 2$ mm. Pressure: 10 MPa; $E = 1,000$ MPa; $\nu = 0.3$; $\sigma_y = 10$ MPa. The mesh has 452 nodes and 800 elements. Deformed display in all cases has been multiplied by an amplification factor to help visualization.

7.2 L-shaped test

This benchmark test has the purpose of verifying the behavior of both approaches at the interior corner of the L-shaped domain. The test problem is displayed in Fig. 5. A single

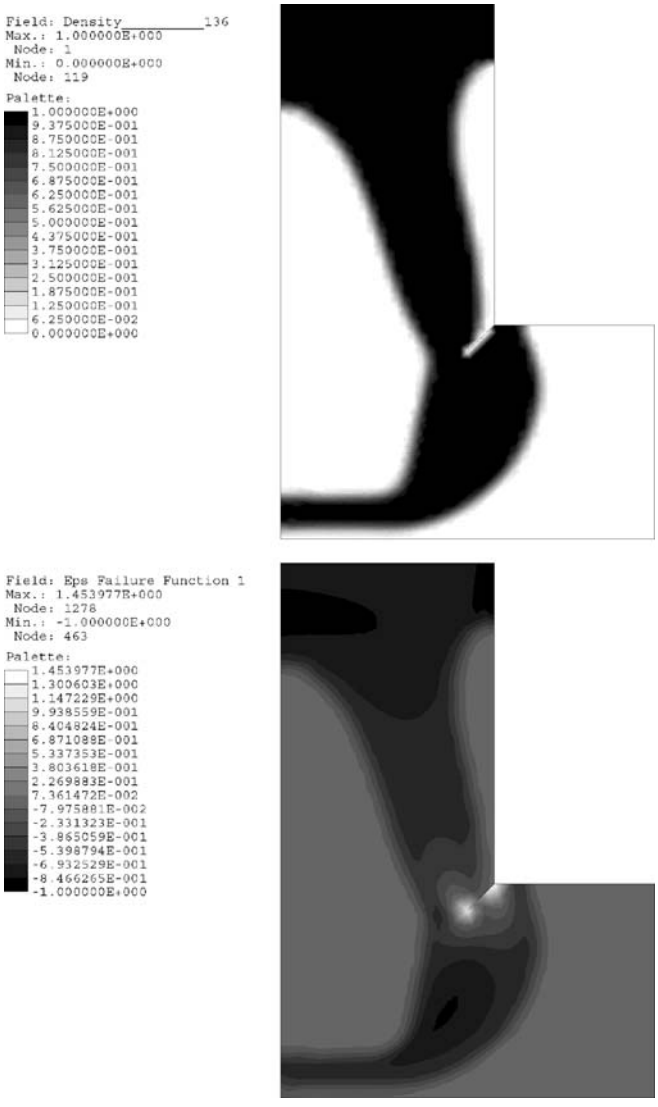

Fig. 8 Strain energy approach. Final design and ε-failure-function distribution

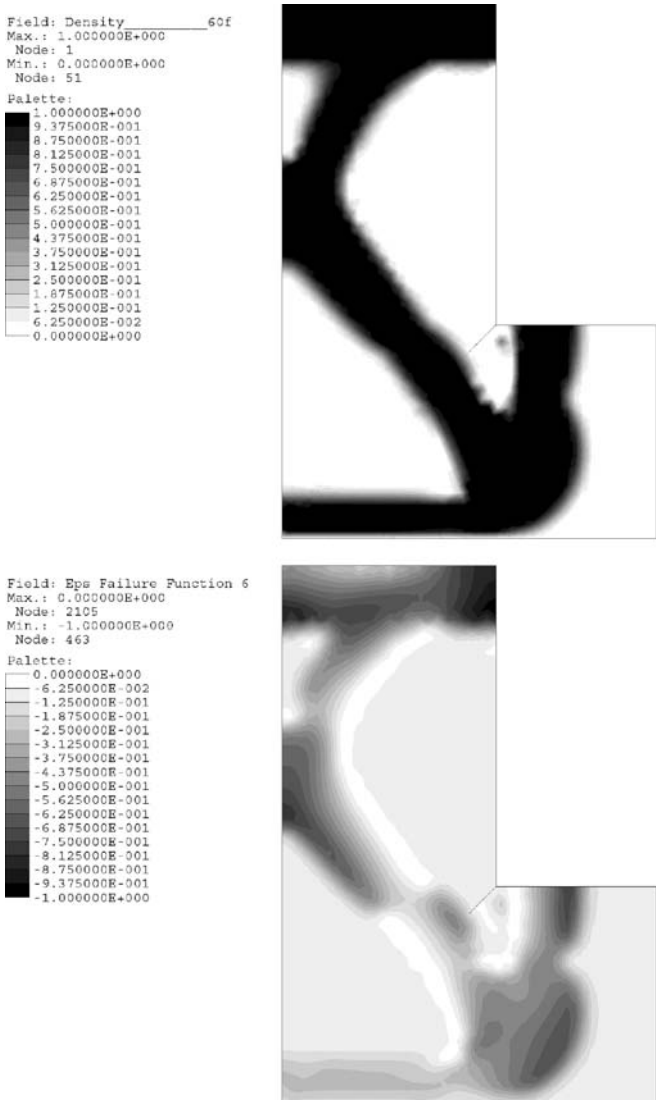

Fig. 9 Minimum mass approach. Final design and ε-failure-function distribution

load pushes the device upward while the contact condition is defined on the lateral support. Before analyzing the corresponding results, a detail concerning the initial setup of this example should be noted. The penalization on the density gradient (20) has been included to inhibit checkerboard and to control the final topology complexity. Moreover, it works like a perimeter penalization. Therefore, the algorithm "prefers" designs attached to the boundaries, as they provoke a reduction in the computable perimeter and, thus, a lower value for the cost function[1]. To avoid this preference, all the nodes belonging to boundaries with a null Neumann condition are set to zero density.

The mesh used has 2,035 nodes and 3,873 elements. Material properties are $E = 2.0 \times 10^5$ MPa, $\nu = 0.3$; $\sigma_y = 700$ MPa. Upper traction is 100 MPa and device thickness $t = 5$ mm. Figures 6 and 7 show the final design for both problems: minimum strain energy and minimum mass, respectively. The minimum mass problem is run first and its minimum value has been used to run the strain approach. Differences, as expected, are appreciable. The strain energy design shows a clear tendency to attach itself to the right boundary to stiffen the design (this attachment has been precluded by construction as previously explained). On the other hand, the mass minimization design tries to avoid stress concentrations and to change the stress flux. Also, the lower horizontal bar is re-designed to ensure parallel contact between piece and foundation and, thus, avoiding concentrated contact stresses. Regularized failure functions for both cases are also shown in Figs. 6 and 7 with expected results.

An extension of this test has been performed by the introduction of a "crack" on the inner corner. Again, all nodes attached to the crack boundary have been set to zero density. Figures 8 and 9 show the final designs. The minimum mass approach gives a final design that completely by-passes the

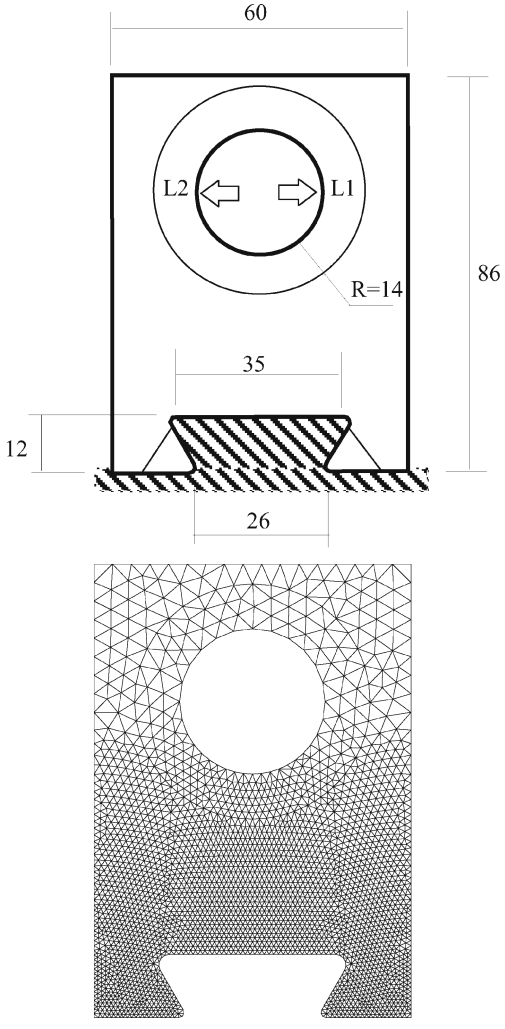

Fig. 10 Dovetail device

[1] This observation was highlighted during a meeting with the TopOpt group at DTU, Lyngby, Denmark.

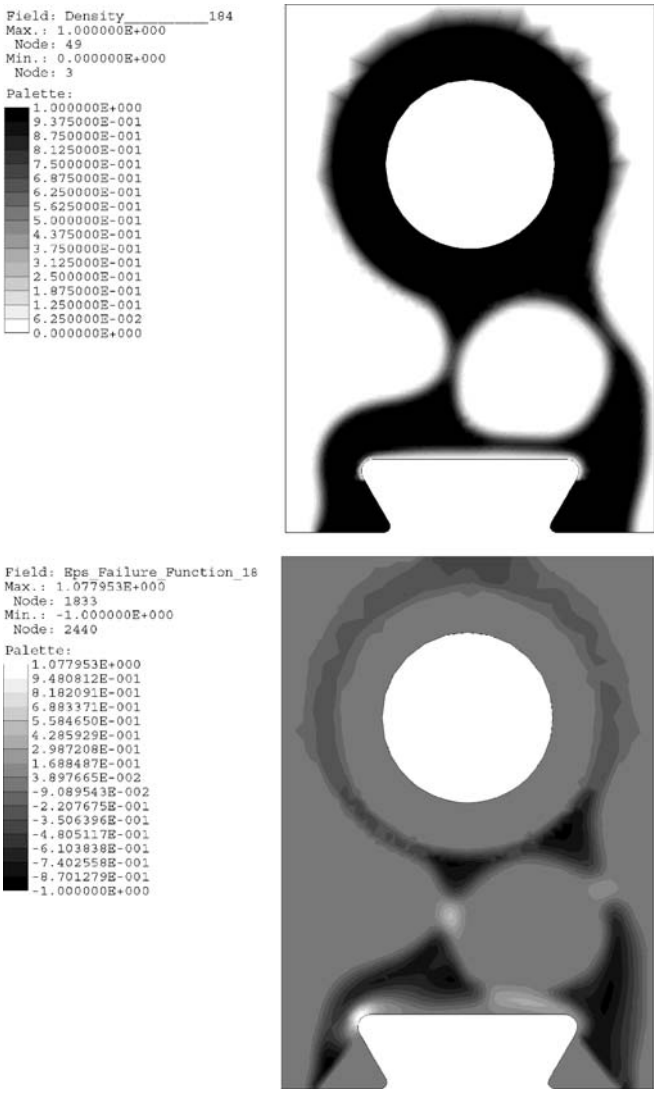

Fig. 11 Single-load case. Final design and ϵ-relaxed failure function for the minimum energy problem

initial crack, while the strain approach persists in the search for the stiffest design.

Focusing the attention on the failure-function distribution of the minimum mass problem (Fig. 9), it is interesting to see that the slanted bar is submitted to a bending distribution that changes its signal. This is put in evidence by the saturated white region that changes sides along the bar. As a consequence, the cross-section with null bending is slightly smaller than the rest of the bar. This behavior has been repeatedly observed in other examples based on the same approach (for a review, see Pereira et al. 2004, Fancello and Pereira 2003).

7.3 Device with a dovetail joint

This example shows a typical mechanical component submitted to two different loads that produce different contact conditions and, consequently, different optimal designs. A search for the minimum mass design has been previously performed in Fancello and Pereira (2003), where the contact problem was circumvented by applying equivalent forces to the dovetail joint. Here, consistent contact conditions are included. Three regions not submitted to optimization were defined: the first one is a ring around the hole and the two others contain the contact surface (differently to previous examples, where the contact region was also considered for optimization). These initial conditions allow us to disregard for the time being possibly contact-stress peaks. Material properties are $E = 210,000$ MPa, $\nu = 0.3$, $\sigma_{adm} = 200$ MPa and the thickness of the device is 40 mm. The loads are $L1 = L2 = 6000$ N (see Fig. 10). The mesh has 2,921 nodes and 5,568 elements The mesh is not completely symmetric, although it seems to be at a first glance.

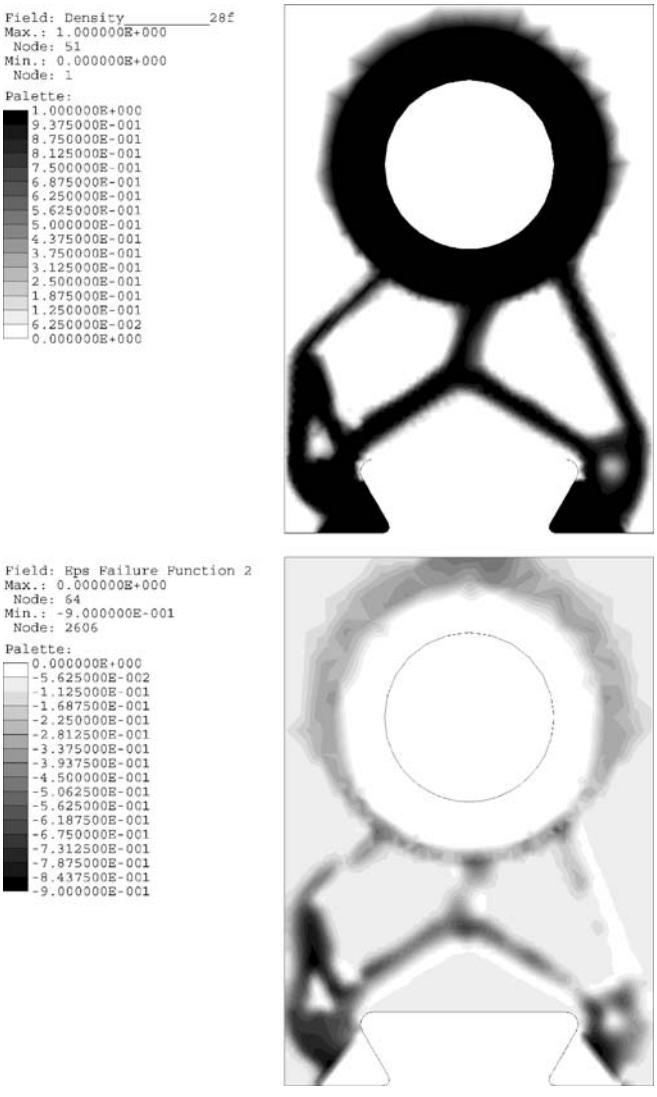

Fig. 12 Single-load case. Final design and ϵ-relaxed-failure function for theminimum mass problem

Fig. 13 Multiple-load case, minimum energy problem. Final density

The single-load case L1 is analyzed first. Figure 11 shows the final design and corresponding regularized failure function for the minimum energy problem. Analogously, Fig. 12 shows the final design and regularized failure function for the minimum mass problem. Final designs are, as expected, non-symmetric and present quite different geometries. It is worth noting that the mass obtained in the minimum mass problem was used as a constraint for the minimum compliance problem.

Both loads L1 and L2 were independently applied in the second test. The objective function of the minimum energy problem was defined as the equally weighted sum of the energy of each load. Conversely, the minimum mass problem included the effect of each load as an independent set of stress constraints. Figures 13 and 14 show the final design and failure functions for the minimum energy problem, while Figs. 15 and 16 show equivalent results for the minimum mass problem. Differences in both designs are evident and, as expected, results from the minimum strain energy approach present no satisfaction of the failure function in some regions.

It is worth noting that these designs should be symmetric, a property that is partially accomplished if we compare them with those of the single-load case (Figs. 11 and 12). However, lack of perfect symmetry is easily verified mainly in the case of the minimum mass problem. This behavior has been previously noticed in linear models (i.e., no contact), but it is numerically perceptible that the introduction of the contact condition increases the possibility of achieving different local optimum designs at each side of the component due to small numerical asymmetries during the optimization sequence. This behavior is, indeed, accentuated in the minimum mass problem that, due to the stress constraints, presents a less stable behavior than that of the minimum energy model.

8 Discussion and final comments

The inclusion of contact boundary conditions in the topology problem of mass minimization with local (stress) failure constraints is addressed in this paper. The numerical results presented show that local optimal designs can be reached by means of the proposed approach. From the computational point of view, the nonlinear contact condition introduced an additional cost much lower than initially expected. The rough shape of the topology is defined at the early stages of the minimization sequence and, thus, the initial displacement estimate for the Newton algorithm is, in most cases, almost the converged solution. In other words, only a couple of Newton iterations are commonly needed to reach equilibrium after a design change during the optimization process. On the other hand, the contact condition introduces severe changes in the nature of the problem Haslinger and Neittaanmäki (1996). Numerical observation indicates the huge set of local minima

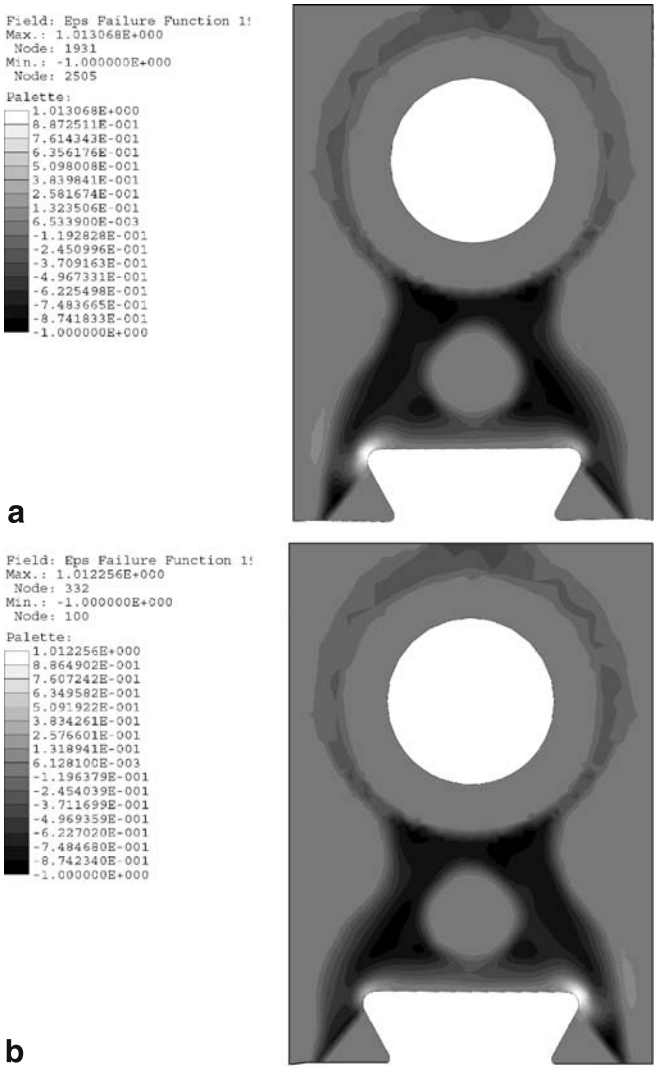

Fig. 14 Multiple-load case, minimum energy problem. **a**-failure-function load 1, **b** ϵ-failure-function load 2

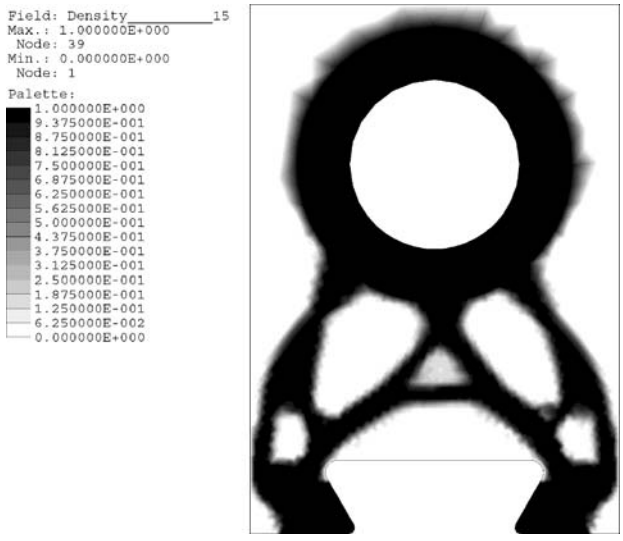

Fig. 15 Multiple-load case, minimum mass problem. Final density

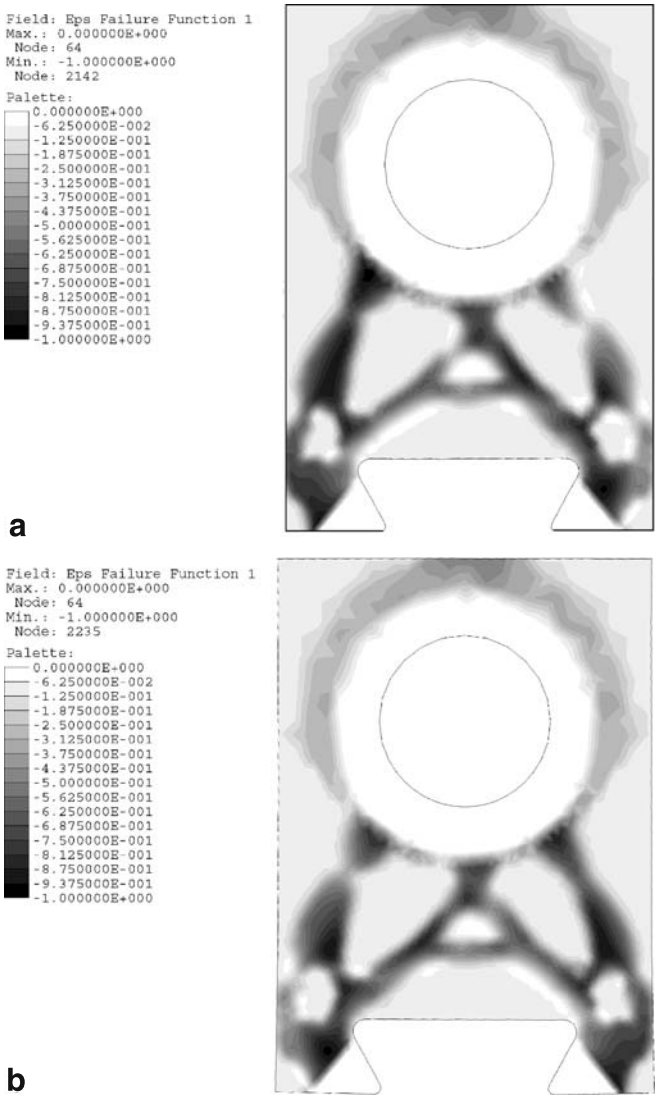

Fig. 16 Multiple-load case, minimum mass problem. **a** ϵ-failure-function load 1, **b** ϵ-failure-function load 2

introduced by the contact condition; the size of the contact region as well as its position (see, for example, the L-test) is influenced by initial density distribution as well as by algorithmic parameters like initial penalization on stress or volume. This fact is related with the lack of differentiability previously mentioned. Different contact distributions drastically change the gradient directions, driving to different local solutions.

Another issue addresses the contact stress distribution. It is clear that the approach proposed here introduces indirectly a limit on the contact stresses. It is possible to see in examples 7.1, 7.2a, and 7.2b that for the given contact boundary shapes and initial setting of the problem, admissible topologies were found that avoid contact stresses above a threshold. However, the existence of solutions (or the ability to find them) in the case of arbitrary contact shapes does not seem to be an easy task. The ability to control contact stress distributions through topology modifications deserves more specific attention. In addition, it is the opinion of the author that an efficient approach should integrate topology and contact shape control of the type seen in, for example, Haslinger and Neittaanmäki (1996), Fancello and Feijóo (1994), Fancello et al. (1995).

As already pointed out in previous works (Pereira et al. (2004); Fancello and Pereira (2003)), the Augmented Lagrangian technique was suggested to solve this problem as an attempt to introduce the failure constraints in a "smooth" way, to reduce the costs of gradient computation and to provide an automatic procedure for the selection of active constraints. Nevertheless, the inherent difficulties of the problem persist. Failure constraints are highly sensitive and the minimization sequence may drive to design points for which the update procedure of Lagrangian multipliers compute non-reasonable high values and no convergence is obtained. Numerical tests showed that better behavior is achieved when the inner minimization problem of the Augmented Lagrangian sequence is performed within a moving box (trust region) smaller than that given by the side constraints of the nodal densities. When the minimum is attained and multipliers are updated, the trust region is centered at the new point and the problem starts again.

It was also noted that problems like the block under compression (that is conceptually analogous to that of a bar in traction) converges much more easily than that of the L-shaped problem, a fact that it is quite reasonable; in the first case, the starting point is feasible and the design space is wide enough to accommodate optimal designs without stress concentration regions. In the L-shaped domain, the initial design is unfeasible and the available room acts as an additional constraint to find a feasible optimal solution.

Concerning numerical costs, a typical run for the L-shaped problem consumes 40 Lagrangian iterations (inner minimization problems) each of which takes an average of

150 solutions of the state equation. These costs may be unacceptable for large-scale problems.

It should be noted also that for the present mass minimization problem, it is easy to formulate examples with no admissible design (i.e., empty design space), which is in contrast to the classical problem of compliance or strain energy minimization.

Despite all the mentioned difficulties, it is interesting to highlight the differences in the final solutions obtained by the most common topology problem and those obtained with the present one. In practical structural design, local (or quasi-local) constraints are a usual requirement, and there is still a lack of different efficient alternatives for including them in topology procedures.

Acknowledgements The author would like to thank the Coordenação de Aperfeiçoamento de Pessoal de Nível Superior—CAPES, and Conselho Nacional de Desenvolvimento Científico e Tecnológico—CNPq, Brazil, which provided partial financial support for this research. He thanks Ana Friedlander Martínez, Sandra A. Santos, and José M. Martínez (IMECC/ UNICAMP) for the optimization algorithm and implementation, and the anonymous reviewer for his contributions on the quality of the presented material.

References

Allaire G, Jouve F, Maillot H (2004) Topology optimization for minimum stress design with the homogenization method. Struct Multidisc Optim 28:87–98

Bertsekas D (1996) Constrained optimization and Lagrange multiplier methods. Athena Scientific, Belmont, MA, USA

Cheng G, Guo X (1997) ε-Relaxed approach in structural topology optimization. Struct Optim 13:258–266

Duysinx P, Bendsøe M (1998a) Topology optimization of continuum structures with local stress constraints. Int J Numer Methods Eng 43:1453–1478

Duysinx P, Sigmund O (1998b) New developments in handling stress constraints in optimal material distribution. In: 7th AIAA/USAF/NASA/ISSMO symposium on multidisciplinary design optimization, pp 1501–1509. American Institute of Aeronautics and Astronautics, Saint Louis, MI, USA, Sept 1988

Fancello E, Feijóo R (1994) Shape optimization in frictionless contact problems. Int J Numer Methods Eng 37:2311–2335

Fancello E, Pereira JT (2003) Structural topology optimization considering material failure constraints and multiple load conditions. Latin American Journal of Solids and Structures 1(1):3–25, http://www.lajss.org

Fancello E, Haslinger J, Feijóo R (1995) Numerical comparison between two cost functions in contact shape optimization. Struct Optim 9(1):57–68

Friedlander A, Martínez J, Santos S (1994) A new trust-region algorithm for bound constrained minimization. Appl Math Optim 30(3):235–266

Haslinger J, Neittaanmäki P (1996) Finite element approximation for optimal shape, material and topology design. Wiley, Chichester, UK

Hilding D, Klarbing A, Petersson J (1999) Optimization of structures in unilateral contact. Appl Mech Rev 52(4):139–160

Hilding D (2000) A heuristic smoothing procedure for avoiding local optima in optimization of structures subject to unilateral constraints. Struct Multidisc Optim 20:29–36

Kirsch U (1990) On singular topologies in optimal structural design. Struct Optim 2:133–142

Pereira JT, Fancello E, Barcellos CS (2004) Topology optimization of continuum structures with material failure constraints. Struct Multidisc Optim 26(1–2):50–66

Petersson J (1996) On stiffness maximization of variable thickness sheet with unilateral contact. Q Appl Math 54(3):541–550

Petersson J, Patriksson M (1997) Topology optimization of sheets in contact by a subgradient method. Int J Num Methods Eng 40(7):1295–1321

Petersson J, Haslinger J (1998) An approximation theory for optimum sheets in unilateral contact. Q Appl Math 56(2):309–325

Simo J, Laursen T (1992) An augmented Lagrangian treatment of contact problems involving friction. Comput Struct 42:97–116

Sokolowski J, Zolesio J (1987) Shape sensitivity analysis of unilateral problems. SIAM J Math Analy 18:1416–1437

Sved G, Ginos Z (1968) Structural optimization under multiple loading. Int J Mech Sci 10:803–805

Wriggers P, Van T, E S (1990) Finite element formulation of large deformation impact-contact problems with friction. Comput Struct 37:319–331